PCCP

Accepted Manuscript

ROYAL SOCIETY OF CHEMISTRY

www.rsc.org/pccp

Plasmonic Color Analysis of Ag-coated Black-Si SERS Substrate

Steven M. Asiala[1], James M. Marr[1], Gediminas Gervinskas[2,3], Saulius Juodkazis[2,3], and Zachary D. Schultz[1]*

1. Department of Chemistry and Biochemistry, Unversity of Notre Dame, Notre Dame, IN, 46556, USA
2. Swinburne University of Technology, John St. Mail, Hawthorn, VIC 3122, Australia
3. Melbourne Centre for Nanofabrication, 151 Wellington Road, Clayton, VIC 3168, Australia

* Email of corresponding author: Schultz.41@nd.edu

Abstract.

Red-Green-Blue (RGB) dark-field imaging can direct the choice of laser excitation for Raman enhancements on nanostructured plasmonic surfaces. Here we demonstrate that black Silicon (b-Si) is a structured surface that has been shown to effectively absorb broad wavelengths of light, but also enables surface enhanced Raman scattering (SERS) when coated with silver (Ag). Coating b-Si with increasing amounts of Ag results in increased dark-field scattering at discrete frequencies associated with localized plasmon resonances. The dark-field scattering was monitored by collecting a far-field image with an inexpensive Complementary Metal Oxide Semiconductor (CMOS) camera, similar to what is available on most mobile phones. Color analysis of the RGB pixel intensities correlates with the observed SERS intensity obtained with either green (532 nm) or red (633 nm) laser excitation in SERS experiments. Of particular note, the SERS response at 633 nm showed low spectral variation and a lack of background scattering compared to SERS at 532 nm. The difference in background suggests sub-radiant (dark or Fano resonances) may be associated with the SERS response at 633 nm and a non-resonant character of SERS. These results indicate that b-Si serves a template where Ag nucleates during physical vapor deposition. Increased deposition causes the deposits to coalesce, and at larger Ag thicknesses, bulk scattering is observed. Comparison with a high enhancement Ag SERS substrate further illustrates that a high density of plasmonic junctions, or hotspots, is important for maximizing the SERS response. The randomness of the b-Si substrate and the corresponding Ag nano-features contributes to a broadband spectral response and enhancement in SERS. Metal-coated b-Si is a promising SERS substrate due to its performance and facile fabrication.

Keywords: Plasmonics, SERS, silicon, sensing, Raman, CMOS

Introduction.

Increased understanding of the electric fields around plasmonic structures has resulted in efforts to develop highly sensitive and reproducible sensors.[1, 2] In particular, the enhancement of Raman scattering from molecules in close proximity to the structures, commonly referred to as surface enhanced Raman scattering (SERS), is particularly attractive. SERS provides chemical information from the unique Raman spectra obtained from molecules, while also improving the sensitivity of Raman to the single molecule level.[3, 4] The application of SERS detection has rapidly expanded to areas including catalysis, forensics, medicine, and environmental sensing.[5-9]

The connection between plasmon resonances and SERS is now well established.[10] There are excellent examples in the literature showing how Raman enhancements track with plasmon resonances.[11, 12] Recent studies have shown that the enhancements around nanostructures can change depending on the plasmon resonance excited.[13, 14] Dark-field scattering is one way to assess the plasmon resonances present.[15] Examination of the plasmon resonances in a SERS substrate can provide insight into the observed enhancements.

There has been significant interest in fabricating SERS substrates that are both reproducible and show a high signal enhancement. A number of routes have been pursued including assembly of nanoparticles,[16] electro- and photochemical deposition,[17, 18] and physical vapor deposition processes.[19-21] In general, a driving design principle is to maximize the number of junctions, or crevices, between plasmonic structures. Interestingly, it has been modeled that geometric homogeneity of the nanostructures is not required for either high or uniform enhancements.[22] Furthermore, it has been shown that aggregation can decrease the SERS response depending on the plasmonic interactions.[23]

Using templates to pattern the formation of nanostructures can results in a reproducible surface. Anodized aluminum oxide (AAO) is one common template that enables growth of nanostructures at fixed distances.[18, 20] In the case of AAO, the template is sacrificed after the nanostructures are formed. Alternative methods include depositing metal onto a grating[24] or other pre-structured surfaces with varied surface morphologies to promote the formation of junctions and crevices.

Black Silicon (b-Si) is an intriguing new material that can be used to template SERS active substrates.[25] High aspect ratio silicon microstructures can be formed by solution etching in hydrofluoric acid,[26] reactive ion etching,[27] or laser ablation.[28] The term "black" is reference to the strong absorptive and anti-reflective properties arising from tapered pillar and pyramidal structures which adiabatically reduce reflectivity of the high refractive index Si (n = 3.5 for visible wavelengths).[26] It has been shown that depositing gold or silver onto these structures produces SERS active substrates.[25, 29, 30] The topography of the surface forms crevices over a large surface area which give rise to the enhanced scattering. It has also been shown that the observed enhancement varies nonlinearly with the numerical aperture (NA) of the microscope objective used, as a significantly larger signal increase at high NA is observed when compared to other reports.[25] One explanation for this increase is stronger focusing of the laser intensity onto the tips of the Si structures, where metal is preferentially deposited. It is important in optimization to match the b-Si needle height with the depth of focus of the objective lens. This NA dependence may also reflect a polarization effect associated with coupling between plasmonic structures.[31]

In this report, we examine changes in the scattering observed from the vapor deposition of Ag onto a b-Si surface (b-Si@Ag). While Ag is prone to oxidation and sulfidation, it also produces the largest enhancements in SERS and can be protected by adsorption of a chemical monolayer for use in chemical sensing. Dark-field microscopy enables us to visualize the scatter from plasmonic structures, which commonly appear red and green. We present a straightforward method of deconstructing a Red-Green Blue (RGB) color image from a common Complementary Metal Oxide Semiconductor (CMOS) camera to analyze preferential scattering in the red and green region of the visible spectrum. This scattering is shown to correlate well to the SERS response observed with red and green laser excitation. Our results suggest a mechanism wherein the deposited Ag nucleates and then coalesces into larger domains with increased deposition. Incorporating atomic force microscope measurements to determine surface roughness demonstrates that a high density of coupled plasmonic structures yields the largest SERS enhancement. Further, the use of b-Si as a template also shows a high level of signal reproducibility.

Experimental.

Black Silicon fabrication. Black-Si was made from a single-side polished p-type ⟨100⟩ orientation Si wafer using reactive ion etching (RIE) process on a Samco RIE-101iPH tool. Substrates were rinsed in isopropanol, dried under nitrogen flow, and loaded into RIE chamber for etching. Surface morphology and spike geometry highly depend on etching parameters such as plasma power, etching gas flow rates, and process pressure. The pyramidal spikes shown in Figure 1 were obtained with RIE power of 150W, SF_6 and O_2 flow rates of 35 and 45 sccm, respectively, a chamber pressure of 1.0 Pa, and 15 minutes of etching time. At the start of the

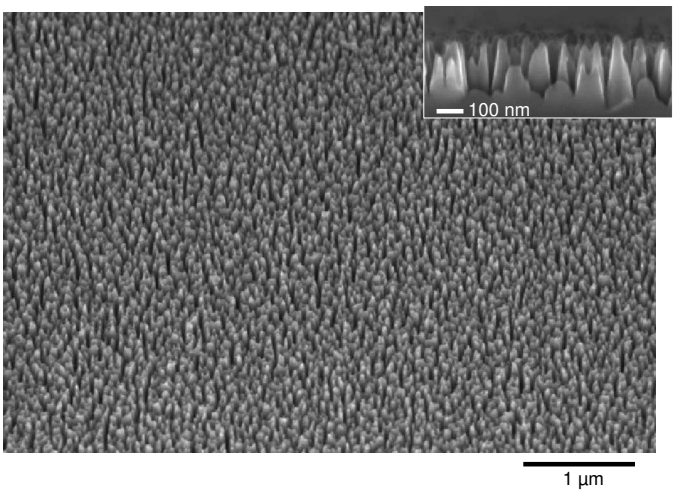

Figure 1. A scanning electron micrograph of the b-Si substrate is shown prior to metal deposition. The surface is shown to consist of heterogeneously spaced pyramidal needles.

RIE process, a self-masking randomly distributes formation of pillars. Pyramidal pillars with a height/width aspect ratio of 2.3 (height=279 nm, tip diameter =16-20 nm) were fabricated onto three-inch wafers.

SERS substrate fabrication. Etched silicon wafers were coated with silver via thermal evaporation. A chromium (Sigma-Aldrich) adhesion layer of variable thickness (1-10 nm) was evaporated onto the b-Si substrate, followed by a silver (Sigma-Aldrich) layer of variable thickness (<100nm). The deposition thickness was monitored by a quartz crystal microbalance. The depositions were carried out at a rate of 0.1 nm/s while rotating the sample stage. The amount of silver deposited onto the b-silicon substrates is denoted by the thickness of the equivalent evaporated film; however, it should be noted the deposits are not necessarily this size. Silver SERS substrates used for comparison were fabricated by thermal evaporation of 500 nm of Ag onto an AAO filter as previously described.[20] The AAO filter is dissolved in 0.1 M NaOH solution to produce a nanostructured Ag film that we used as a reference substrate. All films were stored under vacuum to prevent contamination and oxidation.

SERS substrates were functionalized with by soaking in a 10mM ethanolic solution of thiophenol (Sigma-Aldrich) for 24 h. The substrates were rinsed with ethanol, and allowed to dry prior to measurements.

SERS measurements. Raman spectra were obtained using a lab-built Raman microscope. The microscope is built around an Olympus BX-51 microscope and includes an Andor 303i spectrograph with 300, 600, and 1200 gr/mm gratings and an Andor Newton 970 EMCCD camera. The EM gain was turned off during these experiments. Laser excitation consisted of

either a 532 nm diode laser (Innovative Photonic Solutions) or a 632.8 nm HeNe laser (ThorLabs). The laser power at the sample was attenuated to 1 mW for all measurements. The Rayleigh light was filtered using RazorEdge edge-pass filter (Semrock) at the appropriate wavelength. Excitation and collection of the scattered photons was performed with a Zeiss EC Epiplan-Neofluar 50x reflective dark-field objective (N.A. = 0.8). For Raman measurements, the laser excitation and scattered photons passed through the center of the objective. Sample acquisitions were 10 – 500 ms long. Spectra from 5-10 points on the surface were averaged together for the results shown.

Dark-field microscopy. Wide-field images of the photons scattered from the SERS substrates were collected in a reflective dark-field configuration using the same objective as the Raman measurement above. A 100 W tungsten bulb illuminated the sample. The bulb was used at maximum intensity with the heat shield removed from the lamp housing. Color images were collected using a 1.3 megapixel color CMOS camera (Optixcam Summit Series OCS-1.3). The color observed was corrected to certified white reflectance standard (Labsphere, USRS-99-010) prior to recording the images.

Image analysis was performed using ImageJ (NIH) with the 3D Color Inspector plugin.[32] Dark-field images were decomposed into red, blue, and green channels. The average intensity in each channel was determined.

Atomic Force Microscopy (AFM). AFM images were obtained using a Nanonics MV2000 system running NWS software version 2.3. The tip (Supertips, LTD) consisted of a pulled glass

pipette with a tip apex of 20 nm and a cantilever approximately 150 μm long affixed to a quartz tuning fork. The AFM was operated under ambient conditions.

Results and Discussion.

By correlating the RGB color of the scattering to the Raman excitation wavelength, the preferential conditions for SERS based chemical sensing can be determined. The combination of dark-field microscopy, Raman measurements, and atomic force microscopy (AFM) were used to evaluate the formation and performance of plasmonic structures that arise from depositing Ag onto a b-Si substrate.

Figure 2 shows the dark-field microscopy images collected from b-Si coated with increasing amounts of silver. In Figure 2A, the deposition of 25 nm of Ag results in small, isolated islands of scattered light that can be observed on top the b-Si substrate. It has been reported previously that metal deposition occurs preferentially at the tips of the b-Si structures. The localized points of light on the dark background support this, as the b-Si substrate may absorb light that is not scattered by the metallic deposits. Increasing the amount of Ag deposited to 50 nm (Fig. 2E) further increases the number of locations back-scattering light from the surface. At a deposition thickness of 100 nm (Fig. 2I), the spots appear to coalesce into larger domains producing a reflective mirror surface.

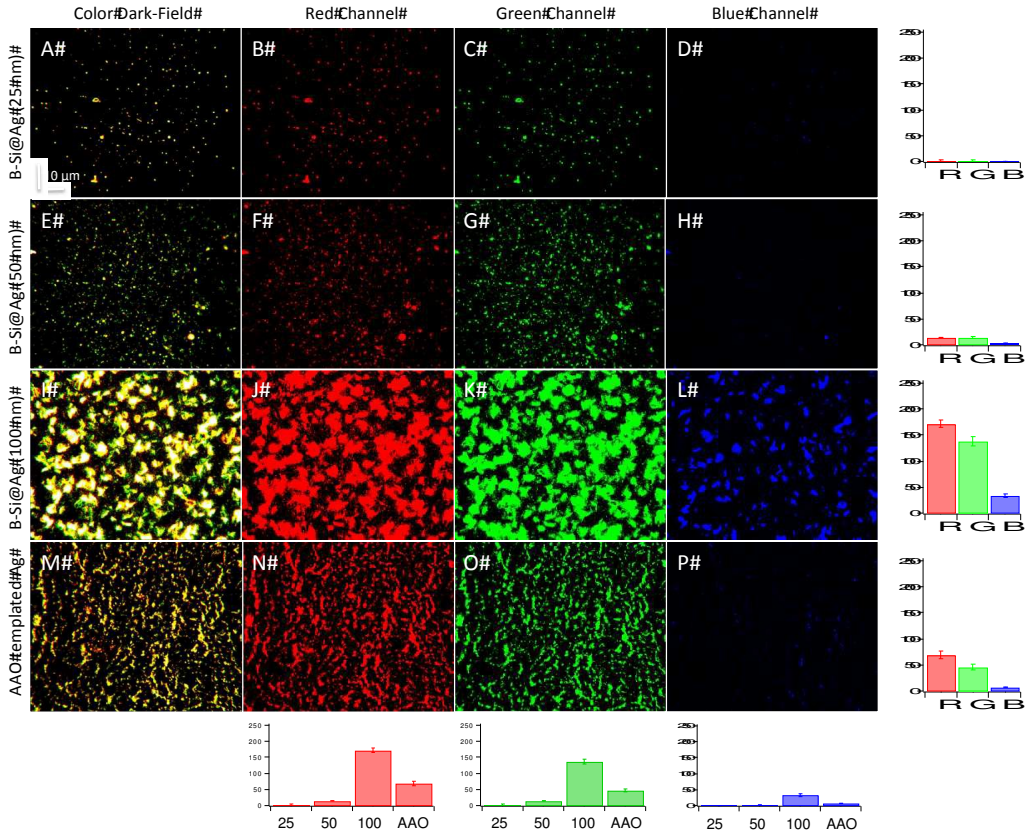

Figure 2. Dark-field microscopy images are shown for b-Si@Ag substrates with 25 nm (A), 50 nm (E), and 100 nm (I) of Ag deposited. The decomposition of the RGB image into the red, green, and blue channels is shown for the indicated thicknesses. For comparison, a reference SERS substrate (M-P) produced by vapor deposition into an AAO template is also shown. The bar graphs at the bottom show the mean scattering intensity from a series of images for each sample in the respective color channel. To the right the relative scattering intensity from each R, G, B channel is plotted for each sample class. All images are the same scale as indicate in panel A.

The observed scattering appears green to yellowish in the raw images. The images were acquired with an inexpensive CMOS camera of lower quality than is available on most mobile phones today. Color images on a CMOS camera are formed from the response of pixels in a color filter array, the most commonly used is the Bayer pattern.[33] The filters associated with the Bayer pattern have broad bandwidths nominally centered at 650 nm (R), 550 nm (G), and 450 nm (B). The contributions of each color pixel in the Bayer filter pattern were decomposed using the 3D Color Inspector plugin for ImageJ. The substrate with 25 nm of Ag shows clear responses from the red and green pixels, but no response in the blue channel. As the amount of Ag is increased, the red and green channels continue to show increased response. At a Ag thickness of 100 nm, in addition to the increased response in the red and green channels, there is also a significant response in the blue channel. The rise of the response in the blue channel appears to coincide with the aggregation of small domains, observed with less silver, into larger domains. At lower coverage, the deposits scatter light, similar to nanoparticles, at discrete frequencies. However, upon coalescing into larger domains, bulk material properties emerge and scattering at all wavelengths is observed. It is noteworthy that the size of the features in the dark-field image does not correspond to the actual size, but merely shows the scattering intensity/efficiency of a particular location. Because of this feature, optical imaging of sub-diffraction limited objects is possible. This property of dark-field imaging is used here to provide an aerial map of hot-spots on the SERS substrate.

To contrast the scattering observed from the deposition of Ag onto b-Si, we also examined a SERS substrate that has shown a high level of enhancement. Previous work has shown that vapor deposition onto an AAO forms heterogeneous nanostructures. Upon dissolution of the AAO template, these nanostructures give rise to a large and uniform Raman

enhancement factor (10^7-10^8).[20] Again, significant scattering is observed in the red and green channels (Fig. 2N-O), but almost no response is observed in the blue channel (Fig. 2P).

Current understanding of the SERS process correlates the wavelength of plasmon resonance and excitation to the observed enhancement.[34] It has been further shown that in aggregated nanoparticles, the existence of dark modes can further enhance signals where scattering is not observed in the far field.[35] The dark-field microscopy results suggest that the b-Si pillars act as nucleation sites for the growth of metallic deposits. Light impinging upon the surface is scattered away from the substrate and observed rather than being adsorbed by the Si. As the metal deposition is increased, the individual patches converge. Percolation of nanostructures is known to change the optical properties of nanomaterials.[36] It has been shown that the aggregation of nanoparticles shifts the plasmon resonances to longer wavelengths.[37] Additionally the spacing between metal nanostructures is important for optimizing the enhancement.[38] Balancing the spacing between converging metallic deposits may allow for controlled formation of hotspots. Thus, modifying the etching conditions to control the initial Si pillar spacing may be a useful strategy to optimize the substrates.

Figure 3 shows representative SERS spectra obtained from both a b-Si@Ag substrate with 50 nm of Ag deposited and the reference Ag substrate with both 532 and 633 nm excitation.

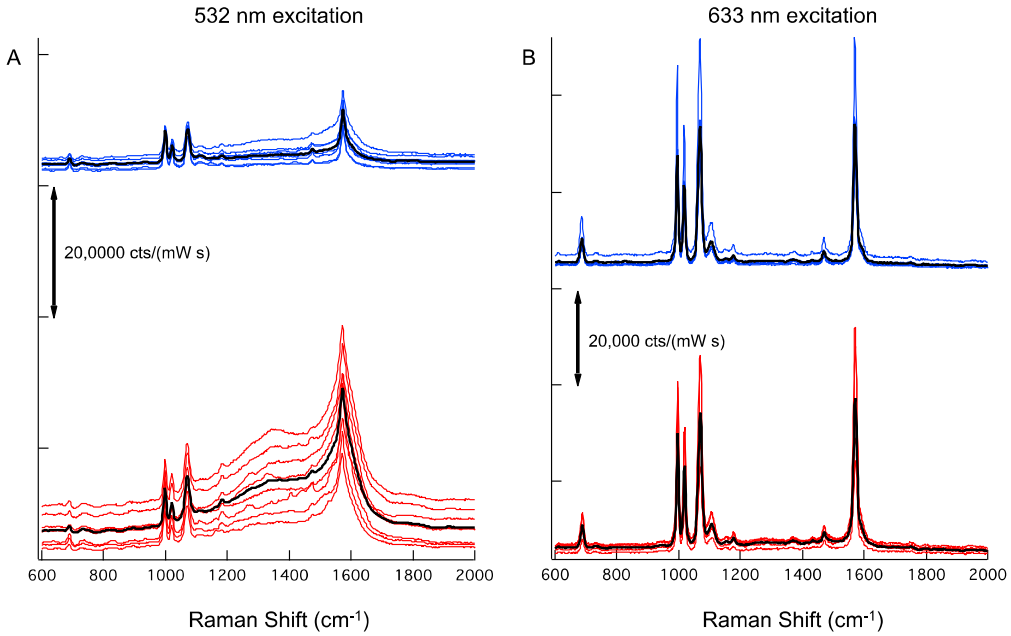

Figure 3. Point Raman spectra obtained from thiophenol on 50nm b-Si@Ag (blue) and Ag SERS (red) substrates are shown at the two excitation wavelengths– 532 nm (n=8, A) and 633 nm (n=5, B). The average spectrum obtained from the sets of spectra is overlaid in black. Sets of spectra from each substrate are offset for clarity.

Similarities and differences are observed in the SERS spectra. In Figure 3A, excitation of the Raman scattering at 532 nm exhibits relatively large standard deviation in the observed Raman intensities from both substrates. The characteristic background scattering typical of SERS is also observed. Less background scattering is observed from the b-Si@Ag substrate, which may result from absorption of the scattered photons by the b-Si substrate.

In Figure 3B, the SERS spectra obtained at 633 nm are notably different. The most striking feature is the complete lack of background typical of SERS spectra. It has been noted that dark resonances can give rise to improved signal to noise ratios in SERS because the plasmon resonance does not give rise to background scattering.[35] Excitation in a Fano-resonance may also produce a similar effect.[13] In addition to showing reduced background, the SERS intensities observed show less deviation. The observed SERS intensities are also more intense, even without accounting for the λ^4 loss that is expected for scattering phenomena. These results indicate that a larger SERS response from these substrates is obtained at 633 nm. The similarities in the SERS response from the two substrates suggest that both substrates have similar plasmonic environments resulting from Ag nanostructures.

Figure 4 shows the average (n=10) SERS response obtained from different spots of a monolayer of thiophenol adsorbed to the SERS substrates. The spectra in Figure 4 were acquired using 633 nm laser excitation. For b-Si substrates, the SERS intensity is shown to increase with the amount of Ag deposited onto the surface. The SERS response from our comparative substrate is also shown, and is significantly more intense than the spectra from the b-Si substrates. The increase in SERS intensity was also observed when using 532 nm excitation, though the magnitude of the signals was lower.

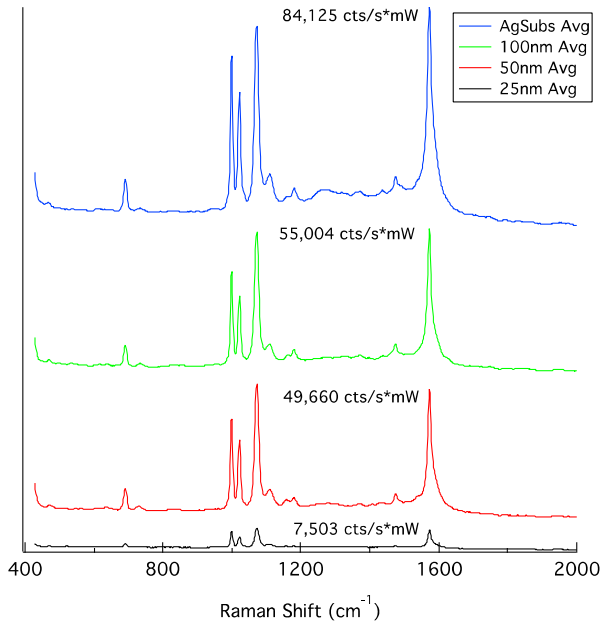

Figure 4. The SERS spectra are shown from b-Si@Ag substrates with 25 nm (black), 50 nm (red), and 100 nm (green) of Ag deposited onto the surface. The spectrum of a Ag substrate using an anodized aluminum oxide template (blue) is also shown. The intensity of the Raman band at 1570 cm^{-1} is reported for each spectrum. The relative SERS intensity is observed to increase with increased metal deposition. The excitation wavelength is 633 nm, and spectra are offset for clarity.

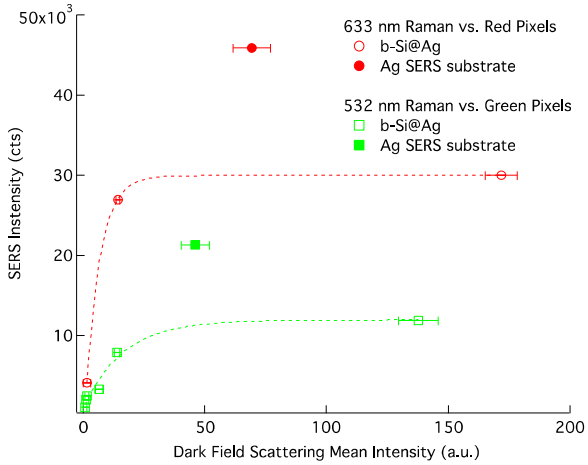

Figure 5. The average SERS intensity obtained from the different substrates is plotted against the mean intensity of pixels in the "red" channel, for 633 nm excitation, and "green" channel for 532 nm excitation. The laser power in both experiments was 1 mW. The b-Si@Ag substrates show an exponential increase in SERS intensity with respect to the dark-field scattering intensity. The dotted lines show an exponential fit to the data. The reference Ag SERS substrate is also shown for comparison. Error bars are shown in both dimensions, the uncertainty in the Raman intensity is less than the size of the markers plotted.

Figure 5 shows the correlation between the observed SERS intensity and the average scattering intensity measured from analysis of the dark-field images. Using 633 nm excitation, the SERS response is observed to increase with the mean intensity of red pixels detected in the dark-field microscopy image. Similarly, the SERS response with 532 nm excitation also increases with the mean intensity of green pixels observed in the dark-field image. An incident power of 1 mW was used for both experiments, clearly indicating the increased SERS response with 633nm excitation. The Bayer filter samples green at twice the frequency of red, which may partially explain why the SERS signal is low relative to the intensity of pixels in the dark-field image. Additionally the spectral response for the red and green channels crosses near 585 nm,[39] which is near the plasmon resonance frequency of aggregated nanoparticles.[40] The reference Ag SERS substrate is known to have broad resonances,[20] but with at least one resonance located in the spectral region that corresponds to red in the Bayer filter pattern.

Interestingly, the SERS responses from our reference SERS substrate (solid symbols) show a higher SERS scattering with less average scattering intensity in the dark-field image. As noted above, the reference spectra showed a minimal response in the blue channel, which suggests preferential scattering at discrete frequencies associated with plasmon resonances. Previous work on this substrate implicated a high density of hotspots giving rise to the high average enhancement.[20] The combination of the SERS intensity and dark-field image analysis suggest a higher ratio of plasmonic particles, or junctions, than was obtained from deposition of Ag on the b-Si.

To further assess the possible role of junctions in the observed SERS response, AFM images were obtained from the substrates. Figure 6 shows the AFM images of 20 μm x 20 μm

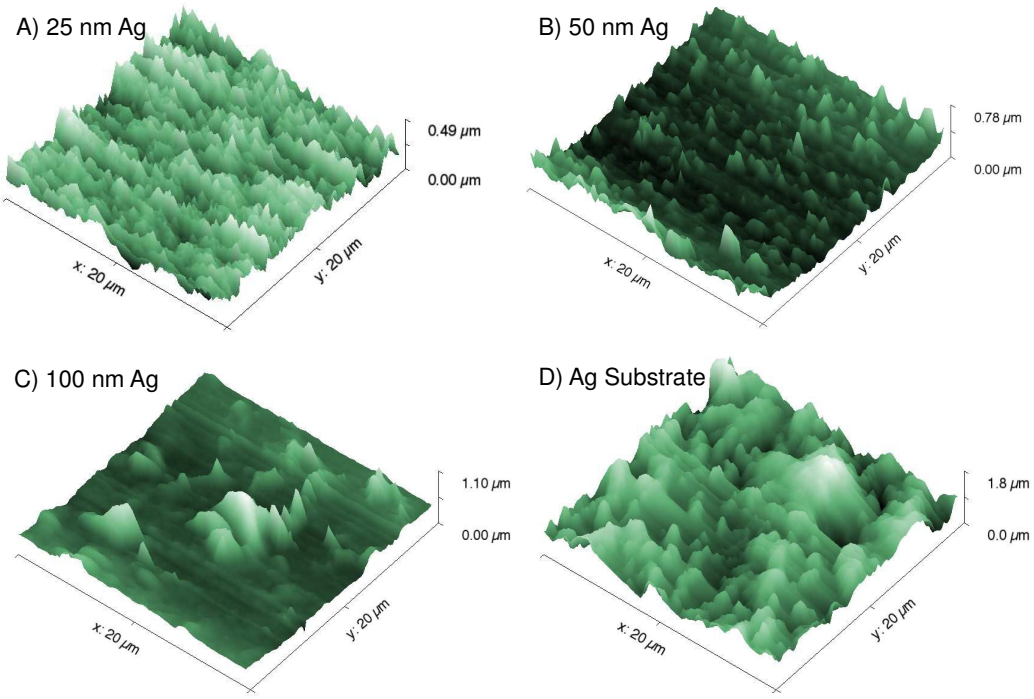

Figure 6. AFM images of the b-Si@Ag substrates (A-C) at the indicated Ag deposition thicknesses and a reference Ag SERS substrate (D) are shown.

sections of the SERS substrates. Similar to the dark-field microscopy, small features are observed on the b-Si@Ag surfaces at low coverage, which become larger as the amount to Ag deposited increases. The height changes observed in the AFM images correspond to about half the thickness of Ag deposited. This agrees with previous reports,[25] indicating that the silver is depositing onto the tips of the Si structures and only partially penetrating to the bottom of the substrate. A similar phenomena was also observed by SEM for the deposition of Au onto b-Si.[41]

To more quantitatively assess the differences in the SERS substrates, we determined the RMS roughness for each substrate in Figure 6. Figure 7 plots the RMS roughness against the SERS intensity observed from the substrates. The SERS intensity at both 633 nm and 532 nm laser excitation is observed to follow a single continuous trend across both the b-Si@Ag substrates and the reference SERS substrate. An increase in surface roughness corresponds to an increase in surface area as measured by cyclic voltammetry on Au-coated laser nano-textured surfaces.[42] However, the most important aspect for SERS is how hot-spots are evolving as the metal film is growing. This study shows that surface roughness at different scales is most important for SERS. Further studies correlating the exact hot-spot location on the dark-field image with the SERS intensity map would deliver insights into SERS mechanisms and selection of the most suitable substrate.

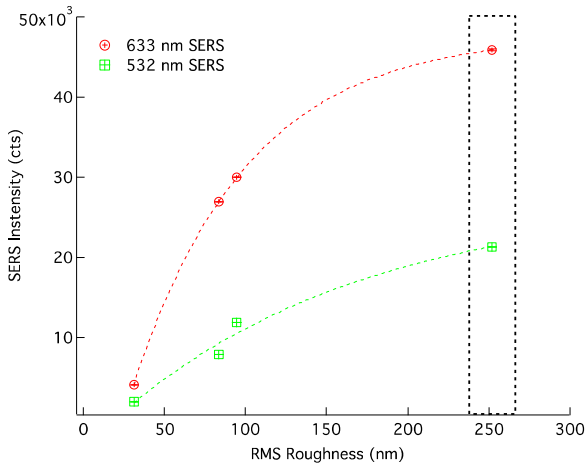

Figure 7. The observed SERS intensity at both 633 nm (red) and 532 nm (green) is plotted against the RMS roughness measured by AFM (Figure 6). The dotted lines are fits of an exponential function to the data. Error bars for the Raman intensity are smaller than the points shown. The data points corresponding to the reference SERS substrate are indicated by the boxed region.

Conclusions.

The results presented illustrate how variable deposition of Ag onto b-Si affects the observed plasmon resonances and observed SERS response. A straightforward image analysis of the dark-field scattering obtained by an inexpensive CMOS microscope camera shows that increased scattering at red wavelengths and the absence of scattering at blue wavelengths gives rise to the largest SERS signal when excited with a red laser. In general, the best SERS signals are obtained by using an excitation wavelength that corresponds to the RGB channel with the largest scattering. The SERS signal obtained with 633 nm excitation showed little background scattering, which suggests that a sub-radiant plasmon resonance may be correlated with the observed SERS signal. This speculative attribution to a sub-radiant mode requires further investigation. Discrepancies between the dark-field scattering and the observed SERS intensity were shown to arise from difference in surface roughness by AFM as greater SERS response was observed for the Ag substrate with the greatest RMS roughness. This reinforces the concept that plasmonic junctions, or crevices, give rise to the larges SERS signals. Overall, these results indicate that tailoring b-Si etching to optimize the density of Ag deposits may provide a route to a reproducible and high-enhancement SERS substrate. Further, a simple color analysis of plasmonic scattering in dark-field image can identify the best excitation wavelength for SERS experiments and predict SERS substrate performance without the use of slower and more costly SEM and AFM characterization methods.

Acknowledgment.

This work was supported through awards from the National Institutes of Health R21 GM107893 and R01 GM109988, a Cottrell Scholar Award from Research Corporation for

Science Advancement, and the Australian Research Council Discovery DP130101205. We are grateful to Pierrette Michaux for developing the black-Si recipe.

References

1. J. P. Camden, J. A. Dieringer, J. Zhao and R. P. Van Duyne, *Accounts Chem. Res.*, 2008, **41**, 1653-1661.
2. N. J. Halas, S. Lal, W. S. Chang, S. Link and P. Nordlander, *Chem. Rev.*, 2011, **111**, 3913-3961.
3. S. Nie and S. R. Emory, *Science*, 1997, **275**, 1102-1106.
4. K. Kneipp, Y. Wang, H. Kneipp, L. T. Perelman, I. Itzkan, R. Dasari and M. S. Feld, *Phys. Rev. Lett.*, 1997, **78**, 1667-1670.
5. I. M. White, S. H. Yazdi and W. W. Yu, *Microfluid Nanofluid*, 2012, **13**, 205-216.
6. K. A. Antonio and Z. D. Schultz, *Anal Chem*, 2014, **86**, 30-46.
7. M. D. Sonntag, J. M. Klingsporn, A. B. Zrimsek, B. Sharma, L. K. Ruvuna and R. P. Van Duyne, *Chemical Society Reviews*, 2014, **43**, 1230-1247.
8. V.-D. Tuan, A. M. Fales, G. D. Griffin, C. G. Khoury, Y. Liu, H. Ngo, S. J. Norton, J. K. Register, H.-N. Wang and H. Yuan, *Nanoscale*, 2013, **5**, 10127-10140.
9. R. A. Alvarez-Puebla and L. M. Liz-Marzan, *Angewandte Chemie-International Edition*, 2012, **51**, 11214-11223.
10. M. Moskovits, *The Journal of Chemical Physics*, 1978, **69**, 4159-4161.
11. A. D. McFarland, M. A. Young, J. A. Dieringer and R. P. Van Duyne, *J. Phys. Chem. B*, 2005, **109**, 11279-11285.
12. A. M. Michaels, J. Jiang and L. Brus, *J. Phys. Chem. B*, 2000, **104**, 11965-11971.
13. J. Ye, F. F. Wen, H. Sobhani, J. B. Lassiter, P. Van Dorpe, P. Nordlander and N. J. Halas, *Nano Lett*, 2012, **12**, 1660-1667.
14. X. Wang, M. H. Li, L. Y. Meng, K. Q. Lin, J. M. Feng, T. X. Huang, Z. L. Yang and B. Ren, *ACS Nano*, 2014, **8**, 528-536.
15. W. S. Chang, L. S. Slaughter, B. P. Khanal, P. Manna, E. R. Zubarev and S. Link, *Nano Lett*, 2009, **9**, 1152-1157.
16. C. J. Orendorff, A. Gole, T. K. Sau and C. J. Murphy, *Anal. Chem.*, 2005, **77**, 3261-3266.
17. R. Alam, I. V. Lightcap, C. J. Karwacki and P. V. Kamat, *ACS Nano*, 2014, **8**, 7272-7278.
18. S. J. Lee, A. R. Morrill and M. Moskovits, *J. Am. Chem. Soc.*, 2006, **128**, 2200-2201.
19. J. D. Driskell, S. Shanmukh, Y. Liu, S. B. Chaney, X. J. Tang, Y. P. Zhao and R. A. Dluhy, *J. Phys. Chem. C*, 2008, **112**, 895-901.
20. S. M. Asiala and Z. D. Schultz, *Analyst*, 2011, **136**, 4472-4479.
21. C. L. Haynes and R. P. Van Duyne, *J. Phys. Chem. B*, 2001, **105**, 5599-5611.
22. Y. Nishijima, J. B. Khurgin, L. Rosa, H. Fujiwara and S. Juodkazis, *Opt. Express*, 2013, **21**, 13502-13514.
23. M. A. Mahmoud and M. A. El-Sayed, *Nano Lett*, 2009, **9**, 3025-3031.
24. X. Deng, G. B. Braun, S. Liu, P. F. Sciortino, B. Koefer, T. Tombler and M. Moskovits, *Nano Lett*, 2010, **10**, 1780-1786.

25. G. Gervinskas, G. Seniutinas, J. S. Hartley, S. Kandasamy, P. R. Stoddart, N. F. Fahim and S. Juodkazis, *Annalen der Physik*, 2013, **525**, 907-914.
26. X. Liu, P. R. Coxon, M. Peters, B. Hoex, J. M. Cole and D. J. Fray, *Energy & Environmental Science*, 2014, **7**, 3223-3263.
27. H. Jansen, M. Deboer, R. Legtenberg and M. Elwenspoek, *J. Micromech. Microeng.*, 1995, **5**, 115-120.
28. T. H. Her, R. J. Finlay, C. Wu, S. Deliwala and E. Mazur, *Applied Physics Letters*, 1998, **73**, 1673-1675.
29. R. Buividas, P. R. Stoddart and S. Juodkazis, *Annalen der Physik*, 2012, **524**, L5-L10.
30. A. Chou, E. Jaatinen, R. Buividas, G. Seniutinas, S. Juodkazis, E. L. Izake and P. M. Fredericks, *Nanoscale*, 2012, **4**, 7419-7424.
31. S. Juodkazis, L. Rosa and Y. Nishijima, in *Nanoplasmonics*, CRC Press, 2013, DOI: 10.1201/b15622-4, pp. 57-111.
32. C. A. Schneider, W. S. Rasband and K. W. Eliceiri, *Nature Methods*, 2012, **9**, 671-675.
33. 1976.
34. P. L. Stiles, J. A. Dieringer, N. C. Shah and R. R. Van Duyne, *Annu Rev Anal Chem*, 2008, **1**, 601-626.
35. K. L. Wustholz, A.-I. Henry, J. M. McMahon, R. G. Freeman, N. Valley, M. E. Piotti, M. J. Natan, G. C. Schatz and R. P. V. Duyne, *J. Am. Chem. Soc.*, 2010, **132**, 10903-10910.
36. M. Gaio, M. Castro-Lopez, J. Renger, N. van Hulst and R. Sapienza, *Faraday Discuss*, 2015, **178**, 237-252.
37. B. M. Reinhard, M. Siu, H. Agarwal, A. P. Alivisatos and J. Liphardt, *Nano Lett*, 2005, **5**, 2246-2252.
38. K. D. Alexander, K. Skinner, S. P. Zhang, H. Wei and R. Lopez, *Nano Lett*, 2010, **10**, 4488-4493.
39. Z. Sadeghipoor, Y. M. Lu and S. Susstrunk, *Digital Photography Viii*, 2012, **8299**, 14.
40. A. M. Moran, J. H. Sung, E. M. Hicks, R. P. Van Duyne and K. G. Spears, *J. Phys. Chem. B*, 2005, **109**, 4501-4506.
41. G. Seniutinas, G. Gervinskas, R. Verma, B. D. Gupta, F. Lapierre, P. R. Stoddart, F. Clark, S. L. McArthur and S. Juodkazis, *Optics Express*, 2015, **23**, 6763-6772.
42. R. Buividas, N. Fahim, J. Juodkazytė and S. Juodkazis, *Appl. Phys. A*, 2014, **114**, 169-175.